


# Comparison of PSH results with historical macroseismic observations at different scales. Part 2: application to South-East France

A. Rosti<sup>1</sup> · M. Rota<sup>2</sup> 

Received: 20 September 2016 / Accepted: 14 May 2017 / Published online: 25 May 2017  
© Springer Science+Business Media Dordrecht 2017

**Abstract** The companion paper by Rota and Rosti (Bull Earthq Eng, 2017) illustrates a methodology for comparing PSH results with historical macroseismic observations at different scales, in terms of mean damage. This paper presents examples of application of the methodology, at the different considered scales, to the South-East quarter of France. This moderate seismicity region is characterised by a long history of civilization, which makes macroseismic observations available for a long time span, although they are highly approximated measures of the seismic action and they are affected by significant uncertainties. The first scale of application presented is at a single site, i.e. the city of Annecy. This example shows that, despite the seismic history of this city is characterised by a significant number of macroseismic observations spanning over a long time period, they mostly consist of very low intensity values and hence the comparison at a single site is not very meaningful. Therefore, the comparison is carried out on a set of seven aggregated sites, well distributed in the region of interest, providing interesting results and suggesting the opportunity of extending the comparison at an even larger scale. The comparison at the regional scale also allows some interesting observations, although it is obviously able to only provide general (average) indications on the PSH results. These comparisons were aimed at showing the applicability of the proposed methodology, pointing out advantages and drawbacks of the different application scales.

**Keywords** Fragility curves · Macroseismic observations · Probabilistic seismic hazard analysis · Sampling in space · South-East France · SisFrance database

---

✉ M. Rota  
maria.rota@eucentre.it

<sup>1</sup> ROSE Programme, UME School, IUSS Pavia, Via Ferrata 1, 27100 Pavia, Italy

<sup>2</sup> European Centre for Training and Research in Earthquake Engineering, Via Ferrata 1, 27100 Pavia, Italy

## 1 Introduction

Recent examples of large and destructive earthquakes occurring in places mapped as having relatively low hazard, and hence producing shaking much greater than predicted by the hazard maps, sparks debates concerning the need for verification and/or validation of the ground motion intensity estimates provided by probabilistic seismic hazard (PSH) analysis studies (Iervolino 2013). Indeed, as discussed for example by Stirling and Petersen (2006), overestimating seismic hazard of an area may lead to an unnecessary increase of the building construction costs. Conversely, underestimating seismic hazard may result in engineers and planners being unprepared in front of the effects of a major earthquake, which would produce unexpectedly high consequences in terms of costs and victims.

Stein et al. (2011) noticed that, surprisingly, although hazard maps are widely used in many countries, very often their results have not been objectively tested. Despite research focused on objective testing of PSH models has been progressing for some years (e.g. Stirling 2012) and several initiatives have been launched to test earthquake forecast around the world (e.g. the Collaboratory for the Study of Earthquake Predictability, CSEP, the Global Earthquake Model, GEM, and the Yucca Mountain seismic hazard modelling efforts), there are currently no generally agreed upon criteria for judging the performance of a PSH map.

Different types of observations can be used for the comparison with seismic hazard results, including accelerometric data (e.g. Ordaz and Reyes 1999; Albarello and D'Amico 2008; Stirling and Gerstenberger 2010; Tasan et al. 2014), “synthetic” accelerations (e.g. Ward 1995; Tasan et al. 2014), macroseismic intensities (e.g. Stirling and Petersen 2006; Labbé 2010) and fragile geological structures (e.g. Purvance et al. 2008; Baker et al. 2013). To this end, the use of independent data, i.e. data not directly included in the PSH, whenever available, should be preferred to allow meaningful comparisons (Beauval 2011).

A multi-scale methodology for comparing the results of PSH with macroseismic observations was proposed in the companion paper by Rota and Rosti (2017). This paper presents some applications of the proposed methodology, at different scales, to illustrate the different steps of this approach and highlight advantages and drawbacks of the selected procedure. The area of study considered for the application consists of the South-East quarter of France. The choice of France for the application derives from the fact that it is an example of moderate seismicity region, for which the interest towards the improvement of PSH studies is demonstrated by the recent establishment of a very comprehensive project, the Sigma project, financed by the scientific and industrial community in France. The project was aiming at improving the knowledge on PSH methodologies and the reliability of PSH results, by obtaining robust and stable estimates of the seismic hazard in France, by means of a better characterisation of the uncertainties involved.

The multi-scale methodology discussed in Rota and Rosti (2017) was hence developed within the framework of the project Sigma. The approach is based on the use of macroseismic intensity observations, starting from the consideration that, in France, more or less reliable historical records, in terms of values of macroseismic intensity, are available on a rather long period of time (around a millennium) and these could be used for comparisons with the results of PSH. However, metropolitan France is characterised by a relatively low seismicity, if compared to other European countries, and this explains the availability of a limited number of events producing intensity observations corresponding to some structural damage. This obviously strongly affects the results of the comparison at single sites, as shown by the example application reported in this paper. For these reasons, the

comparison was also carried out on a set of seven aggregated sites, located in the South-East of France, taking advantage of the assumption of ergodicity of the process of earthquakes' occurrence, which allows sampling in space. Finally, a larger scale was considered, including the entire region of interest. In this case, a grid of points was identified, covering the South-East of France and stochastic fields of ground motion were simulated to generate synthetic acceleration values, compatible with the historical observations.

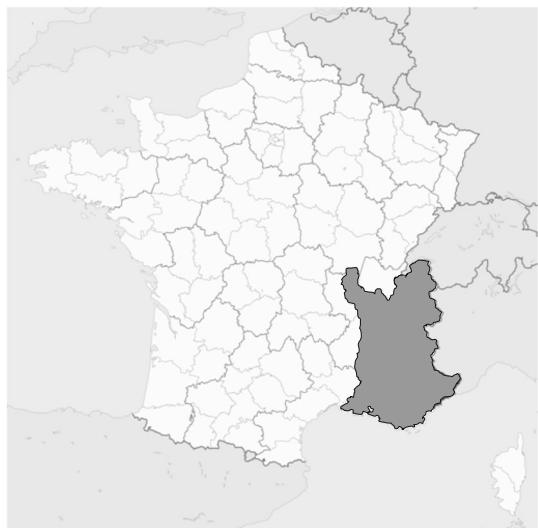
It is important to remark that this work does not aim at validating the results of PSH, but simply at comparing them with macroseismic observations and commenting on the results of this comparison. Moreover, the focus of the paper is not on the results obtained, which are obviously affected by the several assumptions considered in the approach, but on showing the applicability, at the different scales, of the methodology proposed by Rota and Rosti (2017).

## 2 Area of study, relevant building typologies and relative diffusion

The area of study was identified as the South-East quarter of France (dark grey area in Fig. 1), which includes eleven departments, consisting in Alpes Maritimes, Hautes-Alpes, Haute-Savoie, Vaucluse, Savoie, Isère, Rhône, Drôme, Alpes de Haute-Provence, Bouches du Rhône and Var.

To convert macroseismic intensities into mean damage values, information is needed on the building stock existing in the area at the time of the historical events generating the observations. This information is also needed to select appropriate typological fragility curves, which are necessary for converting PGA values into mean damage values. Hence, for a number of sites located in the area, information regarding the building stock, its evolution over time, the history and the urban development was collected, taking advantage of all possible sources of information. However, the collected information resulted to be general and not very useful for a precise identification of building typologies at the time

**Fig. 1** Map of metropolitan France, with identification of the area of study (*dark grey*)



of the historical observations. Hence, for each site, the identification of building typologies was carried out based on expert judgement.

In the South-East quarter of France, the historical building stock is mainly constituted by undressed stone masonry buildings with flexible floors. The four structural typologies reported in Table 1 were identified as of interest, differing by the number of storeys (i.e. 1–2 storeys and more than 2 storeys) and the presence or absence of tie-rods and tie-beams. Their relative diffusion in the area depends on the environmental context of the site. Three different categories were considered, i.e. larger cities, smaller villages and villages in the Alps. For each category, weights were attributed to each of the four considered structural typologies (Table 2). These weights were defined based on the information collected, making large use of expert judgment, considering for example that larger cities are characterised by higher percentages of high-rise buildings with respect to smaller villages and villages in the Alps. Furthermore, higher weights were associated with structural typologies with tie-rods and tie-beams in the larger cities, as these devices are more frequently adopted for the case of taller buildings and for important structures (more diffused in cities).

The assumptions on the subdivision of the building stock at the time of the events, for each considered site, could be obviously improved, whenever more refined information would be available. As an alternative, Riedel et al. (2015) proposed a simplified methodology for assessing vulnerability, starting from very poor information on the building stock (age of construction and number of stories). Although promising, this methodology includes many assumptions, whose reliability should be further tested.

### 3 Conversion of macroseismic intensities into mean damage values

#### 3.1 Available macroseismic observations

Macroseismic observations for the study area were retrieved from the online SisFrance database (<http://www.sisfrance.net>), which gathers parametric information on French historical seismicity over about a thousand years (although the time span for the catalogue

**Table 1** Relevant building typologies for the area of study

Typology	Description	No. of storeys
1	Undressed stone masonry—flexible floors—w/ tie-rods and/or tie-beams	1–2
2	Undressed stone masonry—flexible floors—w/o tie-rods and tie-beams	1–2
3	Undressed stone masonry—flexible floors—w/ tie-rods and/or tie-beams	>2
4	Undressed stone masonry—flexible floors—w/o tie-rods and tie-beams	>2

**Table 2** Weights attributed to the identified building typologies, depending on the environmental context

Environmental context	$W_{Typ. 1}$	$W_{Typ. 2}$	$W_{Typ. 3}$	$W_{Typ. 4}$
Larger city	0.05	0.50	0.15	0.30
Village in the Alps	0.10	0.60	0.10	0.20
Smaller village	0.10	0.70	0.05	0.15

completeness is significantly shorter). The database, which is described in Scotti et al. (2004), provides, for each event, date and time of the earthquake, nature of the shock (e.g. mainshock, foreshock, aftershock, etc.), epicentral location (with an associated reliability index) and epicentral intensity. In addition, for each event, a macroseismic data table lists all the sites where the earthquake has been felt, with macroseismic observations expressed in the MSK-64 intensity scale (Medvedev et al. 1964). A different code is attributed to each macroseismic intensity, according to the reliability of the information linked to the observation.

For the considered study area, the database includes 711 events causing observations, most of which have epicentral intensity smaller than or equal to 5, corresponding to no damage. 603 of these events have epicentre located in France, 108 outside France. Considering also the nature of the shock, there are 89 mainshocks with epicentre in France and with epicentral intensity at least equal to 6, causing macroseismic observations in the study area.

The number of macroseismic observations with intensity at least equal to 6 (corresponding to slight damage in the MSK scale), is about 14% of the total (i.e. 640 out of 4573 observations), confirming that the large majority of the reported macroseismic observations corresponds to intensity values too low to be of any engineering interest. They were produced by 107 independent events. Among these observations, 475 are due to French events (12.1% of the 3928 observations due to French events), whereas 165 are caused by foreign events (25.6% of the 645 observations). This calls for the need of homogenisation of the data related to events occurring at the borders since, according to Rovida (2013) and Scotti (2013), SisFrance and the databases of neighbouring countries (e.g. the Italian macroseismic database DBMI1, Locati et al. 2011) provide different intensity evaluations, which go behind the use of different macroseismic scales.

Figure 2 shows a subdivision of the 107 independent events based on the period of occurrence. The first event, for which intensities at least equal to 6 were observed, corresponds to the 23rd of June 1494 earthquake, with epicentre in the Alps Niçoises. Observation of the plot suggests that the database is very likely to be incomplete in time. Indeed, the number of events increases exponentially with time, which is not physically realistic, unless it indicates a lack of information on older events, not reported in the catalogue. Values of macroseismic intensity observed in the selected area and caused by independent events are shown in Fig. 2 (right).

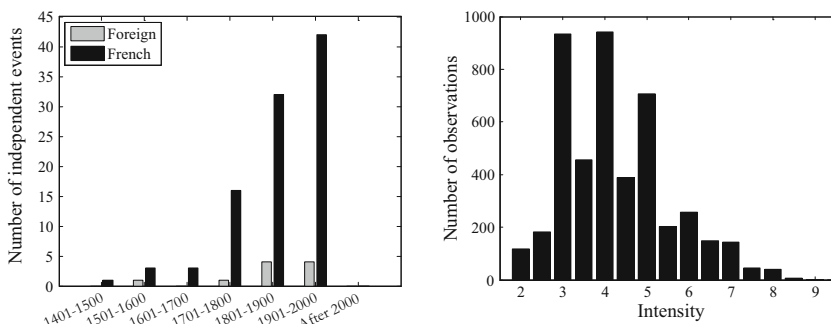


**Fig. 2** Number of independent events causing observations with intensity at least equal to 6 in the study area, for different time intervals (*left*) and statistics of the corresponding macroseismic intensities

### 3.2 Consideration of uncertainty on macroseismic observations

The French macroseismic database SisFrance reports indications on the reliability of each macroseismic observation, based to the quality of the information. Code A means that the reported macroseismic intensity value is certain, code B denotes a fairly certain intensity, whilst code C corresponds to an uncertain intensity value.

To account for these uncertainties, the intensity values were converted into weighted discrete distributions of values, centred on the reported intensity and depending on the reliability of the observations. In case of reliability code A, only the reported intensity value was considered. In case of code B, the reported intensity value,  $I$ , and the intensity levels  $I \pm 0.5$  were taken into account. In case of code C, the reported macroseismic intensity value,  $I$ , and the intensity levels  $I \pm 0.5$  and  $I \pm 1$  were considered. The weights of each discrete intensity level were defined based on normal distributions, centred on the reported intensity, with a standard deviation equal to 0.25 for code B and 0.50 for code C (Fig. 3).

Each weight (Table 3) was calculated by integrating the area subtended by the normal distribution and bounded by the midway percentiles with respect to the selected intensity level.

### 3.3 Conversion of macroseismic observations into mean damage values

As discussed in Rota and Rosti (2017), the macroseismic method proposed by Lagomarsino and Giovinazzi (2006) is used for converting macroseismic intensities into mean damage values. The method accounts for the uncertainty in the attribution of a building

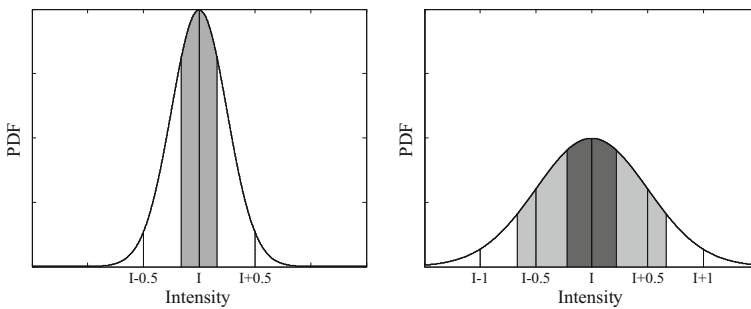


**Fig. 3** Normal distributions centred on the reported intensity level, for reliability codes B (left) and C (right)

**Table 3** Weights attributed to the discrete intensity levels, based on the reliability index

Intensity level	Code A	Code B	Code C
$I - 1$	0	0	0.09
$I - 0.5$	0	0.26	0.24
$I$	1	0.48	0.34
$I + 0.5$	0	0.26	0.24
$I + 1$	0	0	0.09

typology to the EMS-98 (Grünthal 1998) vulnerability classes by defining different values of the vulnerability index.

By only slightly modifying the macroseismic method and assuming the membership function has the meaning of a probability density function, the five vulnerability index values of a given building typology can be defined as percentiles of the membership function and a different weight can be attributed to each of them. In particular, they were defined as corresponding to the 2nd, 16th, 50th, 84th and 98th percentiles. The weights were then defined by integrating the area subtended by the membership function and bounded by the selected percentiles, similarly to what proposed for the uncertainty on the intensity values. This modified definition of the vulnerability indices has the advantage that they are defined in probabilistic terms. Moreover, the attribution of weights based on percentiles has the further practical advantage of obtaining the same weights for different building typologies, provided that the same percentiles are selected.

Figure 4 depicts the membership functions obtained for the four considered building typologies, with the vulnerability indices (diamonds correspond to the median vulnerability index, dots to the 16th and 84th percentiles, whilst squares denote the 2nd and 98th percentiles).

It is noted that building typology 4 of Table 1 was assumed to correspond to the typology M1 of the macroseismic method (rubble stone masonry). The membership functions of typologies 2 and 3 were obtained from that of typology 4, by applying the behaviour modifier for low-rise buildings ( $-0.08$ ) and for the presence of tie-rods and tie-beams ( $-0.08$ ), respectively. They coincide because the values of the two behaviour modifiers coincide. The function for typology 1 was obtained by applying both the low-rise modifier and the one accounting for the presence of tie-rods and tie-beams. As could be expected, the membership function becomes narrower (i.e. reduced range of uncertainty) when additional information on the building typology is added by means of a behaviour modifier. Also, the membership functions of building typologies 1, 2 and 3 are shifted leftward with respect to typology 4, confirming the lower vulnerability of low-rise buildings (typologies 1 and 2) and buildings with seismic devices (typologies 1 and 3). Table 4 reports the values of vulnerability index and the corresponding weights, calculated for the four building typologies of interest. It is noted that, by definition, the weights associated to a given percentile are the same for all building typologies.

By knowing the vulnerability indices of each building typology, it was possible to convert each intensity level into five values of mean damage (Fig. 5). It can be noted that, for a given intensity level, mean damage values are larger in case of mid-rise undressed stone masonry buildings without tie-rods and tie-beams (Fig. 5, right) and the range of

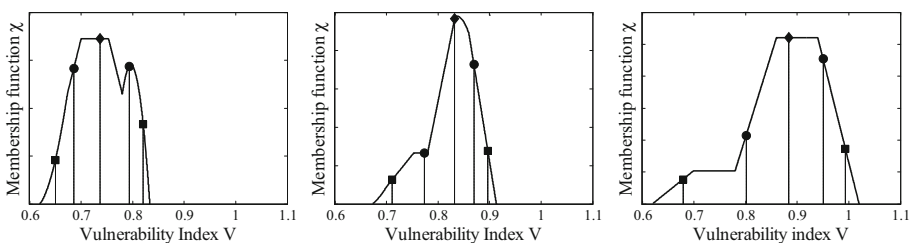


**Fig. 4** Membership functions of typologies 1 (left), 2 and 3 (centre) and 4 (right), with vulnerability indices (diamonds correspond to median vulnerability index, dots to 16th and 84th percentiles, squares to 2nd and 98th percentiles)

**Table 4** Values of vulnerability index for the four considered building typologies and corresponding weights

Vulnerability index	Typ. 1	Typ. 2 and 3	Typ. 4	Weight
$V_2$	0.65	0.71	0.68	0.09
$V_{16}$	0.69	0.77	0.80	0.24
$V_{50}$	0.74	0.83	0.88	0.34
$V_{84}$	0.79	0.87	0.95	0.24
$V_{98}$	0.82	0.90	0.99	0.09

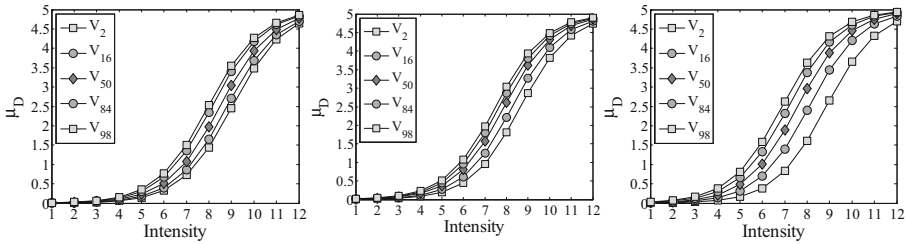


**Fig. 5** Mean damage values versus intensity for the four building typologies of Table 1: typology 1 on the left, typologies 2 and 3 in the centre and typology 4 on the right

uncertainty of mean damage values is wider with respect to the case of low-rise rubble stone masonry buildings with tie-rods (Fig. 5, left).

## 4 Selection of fragility curves for the derivation of mean damage values generated by different PGA levels

### 4.1 Considerations on the selected fragility curves

In the proposed methodology (Rota and Rosti 2017), fragility curves are used to connect the rates of exceedance of PGA levels (obtained from PSH) to mean damage values, to allow the comparison with historical observations. In this case, empirical fragility curves derived from the statistical elaboration of post-earthquake damage data gathered after Italian earthquakes were used. This choice was based on the assumed similarity between the building typologies typical of the South-East French historical building stock and some of the typologies for which Italian post-earthquake damage data are available. Moreover, the use of empirical fragility curves calibrated independent of the French historical macroseismic data was deemed necessary for the implementation of an unbiased comparison.

### 4.2 Considered database of empirical damage data

The considered database of damage data collects information on approximately 140,000 buildings, damaged by six Italian earthquakes occurred in the period 1980–2009. The post-earthquake survey data processed by Rota et al. (2008a, b) were integrated by adding survey data gathered after the event of L’Aquila (2009), including a significant number of data on buildings located very close to the epicentre. The obtained database concerns buildings characterised by a very homogeneous vulnerability, since all data correspond to



events occurred in the Apennines region of Southern-Central Italy. The seismic events considered for the creation of the database consist of Irpinia (1980), Abruzzo (1984), Umbria-Marche (1997), Pollino (1998), Molise (2002) and L’Aquila (2009). Their characteristics, which were retrieved from the parametric catalogue of Italian earthquakes (CPTI 2004), can be found in Rosti et al. (2017).

The data collected after the different events were homogenised and subdivided into several building typologies and damage levels, according to the hypotheses discussed in Rosti et al. (2017). This operation required some assumptions, as the survey forms used for post-earthquake damage data collection evolved with time. Buildings were subdivided into 23 typologies, but only four of these were considered as relevant for South-East France, all consisting of undressed stone masonry buildings with flexible floors (Table 1).

Consistently with the European Macroseismic Scale, five damage grades plus the absence of damage (DS0) were considered: negligible to slight damage (DS1), moderate damage (DS2), substantial to heavy damage (DS3), very heavy damage (DS4) and destruction (DS5). In the derivation of fragility curves, PGA was selected for representing the ground motion. A single value of PGA, evaluated by means of the Sabetta and Pugliese (1987) attenuation law on rock, was attributed to each municipality affected by one of the considered earthquakes. This GMPE was selected because it was derived based on the same earthquakes for which data were available and hence it appeared a consistent choice.

The issue of survey completeness was considered, to obtain an unbiased sample of data, in accordance with Rota et al. (2008a, b). After processing of the available data and considerations on survey completeness, the database finally used for the derivation of fragility curves includes 142,259 usable data, among which 58,408 correspond to the four stone masonry building typologies of interest for the area of study. Figure 6 shows the number of buildings falling in each of the four considered building typologies (left) and the subdivision of these (58,408) data into the different PGA intervals (right).

### 4.3 Derivation of fragility curves and considerations on the results obtained

The derivation of the fragility curves used in this study required the following steps:

- Determination of the Damage Probability Matrixes (DPMs), representing, for each building typology and for each PGA interval, the experimental probability of occurrence of the different damage states.

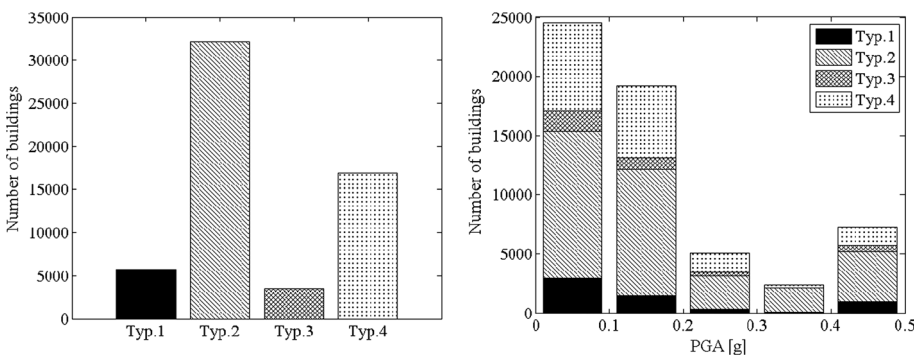


**Fig. 6** Number of buildings for the four considered building typologies (left) and the different PGA levels (right)

- Computation of the probability of exceeding a certain damage state by progressively summing the experimental frequencies from the highest to the lowest level of damage.
- Fitting of the experimental data with a lognormal cumulative distribution by means of the weighted nonlinear regression algorithm of Levenberg (1944) and Marquardt (1963).

Observation of the DPMs corresponding to some typologies highlighted a large predominance of DS1 over the other damage state probabilities, independently from the level of ground motion, particularly for the most vulnerable building typologies (old stone masonry buildings). As discussed in Rota and Rosti (2017), one possible reason for this trend could be the presence of pre-existing damage, which is due to bad maintenance conditions and cannot be ascribed to the seismic event. This pre-existing damage is typically of modest entity, hence mainly affecting the lowest damage levels, and it translates into an unrealistically high percentage of buildings (as high as 90% for the case of typology 1) with damage level DS1 for PGAs lower than 0.05 g. Another possible reason can be related to the issue of survey completeness, which may lead to an underestimation of the percentage of undamaged buildings, particularly in the areas further away from the epicentre, which are hence characterised by low values of ground motion. Based on these considerations, the obtained fragility curves were modified, by ignoring the experimental points in the first PGA interval (i.e.  $PGA = 0.025$  g), which are assumed to be affected by the issues discussed.

Figure 7 reports the fragility curves obtained for the four considered building typologies, which were used in the following parts of this study. Despite the introduced modification, the obtained modified empirical fragility curves still show a trend which is not the typical lognormal shape, indicating that probably the distribution of the empirical data into the different damage and PGA levels does not follow a lognormal model. Alternative models could be hence explored, trying to improve the fitting of the empirical data. Also, despite the removal of the first empirical point (lowest PGA level), the role of pre-existing damage could still be significant and could require further analysis.

#### 4.4 Comparison of the derived mean damage versus PGA curve with observed data

For each considered building typology, the probabilities of reaching different damage levels were computed from the corresponding fragility curves. Under the (commonly accepted) assumption of binomial distribution of damage between the different damage grades (e.g. Braga et al. 1982), it is possible to derive the mean damage curve for each building typology, as a function of PGA:

$$\mu_D = \sum_{k=0}^5 p_k k \quad (1)$$

where  $p_k$  represents the probability of having damage grade  $D_k$  ( $k = 0-5$ ).

The mean damage versus PGA curves of building typologies 2 and 4 were subsequently compared to observed mean damage values, derived from the statistical treatment of the damage data collected after L' Aquila event. Observed mean damage values were derived by fitting a binomial distribution through the observed damage probability matrices and then combining the expected probabilities according to Eq. (1).

For each building typology, Fig. 8 compares the empirically-derived mean damage values (black stars) with the mean damage versus PGA curves, showing a generally good

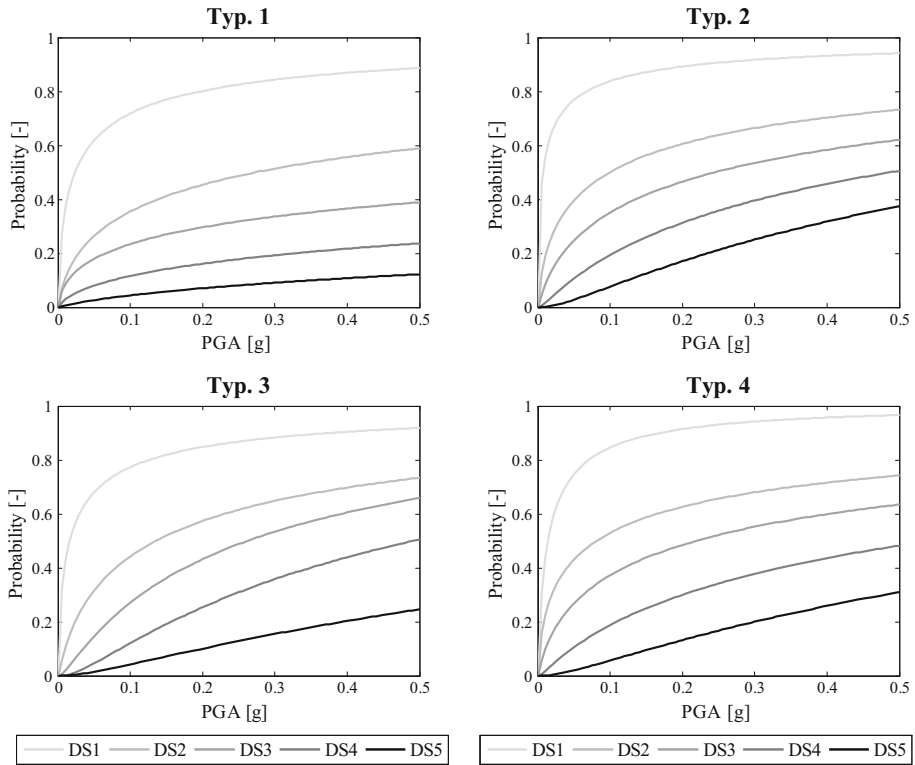


**Fig. 7** Fragility curves adopted for the four considered building typologies

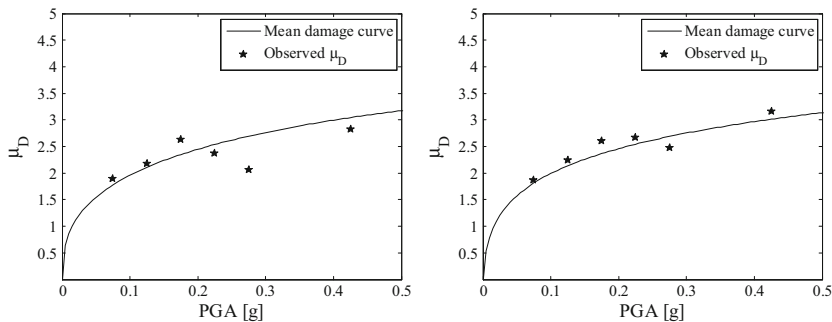


**Fig. 8** Comparison of  $\mu_D$ -PGA curves, derived from the selected fragility functions, with observed mean damage values (black stars). Building typologies 2 (left) and 4 (right)

agreement. It is important to point out that the data used for the derivation of the empirical mean damage values are not independent from those used for the derivation of the fragility curves and this could obviously affect the results of the comparison. Indeed, they are a (small) subset of the database used for the derivation of the curves (Rosti et al. 2017). It would be obviously preferable to use independent data and, possibly, damage data observed in France, to also test the hypothesis of similarity between the Italian building

stock and the typologies diffused in France at the time of the events. However, this was not possible, because limited damage data regarding the French building stock are available and the use of data coming from other regions of the world would pose serious concerns on the similarity between the different building typologies.

## 5 Site-specific comparison

### 5.1 Comparison of PSH results and observations at the site of Annecy

This Section illustrates an example of application of the methodology for comparing PSH results with historical observations to the site of Annecy. Within the study area identified for the applications, the site of Annecy was selected because its seismic history (Fig. 9, left) is characterised by a quite significant number of macroseismic observations with intensity level at least equal to 6, which is the lowest degree for which some minor damage can be expected in buildings, according to the MSK scale.

Each macroseismic intensity value was converted into a weighted distribution of intensity values (Fig. 9, centre), based on the reliability codes reported in SisFrance. Considering its environmental context, Annecy was classified as belonging to “larger cities”. Therefore, according to Table 2, weights equal to 0.05, 0.50, 0.15 and 0.30 were attributed to typologies 1, 2, 3 and 4 of Table 1. This is clearly a simplified assumption, considering that Annecy, at the time of the first considered event (1584) was not yet a large city. A logic tree was then defined, to convert the modified seismic history of Annecy into an equivalent mean damage history (Fig. 9, right), taking into account the four considered building typologies and the five values of vulnerability indices of the macroseismic method, all with their weights. The result is a weighted distribution of mean damage values, for each year corresponding to a seismic event producing macroseismic observations.

For each year, a single mean damage value was then sampled from the corresponding mean damage distribution, using a Monte Carlo approach. Then, for each mean damage level, the observation period was calculated as the difference between 2007, i.e. the last year for which SisFrance provides information, and the first year in which a mean damage value smaller than the selected threshold was observed. Statistics of the best estimate and of the corresponding 90% confidence bounds of empirically-derived annual rates of exceedance were then calculated, as explained in Rota and Rosti (2017).

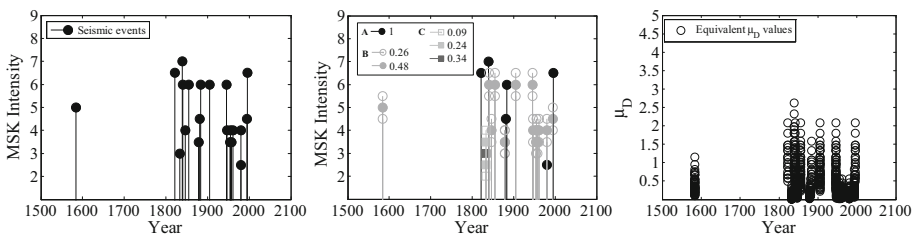


**Fig. 9** Site of Annecy: seismic history (left); seismic history accounting for uncertainty in the intensity values based on reliability codes A, B or C and corresponding weights (centre); resulting mean damage history, presenting a weighted distribution of  $\mu_D$  values for each year in which a seismic event occurred (right)

The different PGA levels from PSH results were converted into mean damage values, using the mean damage versus PGA curve (Fig. 10) derived from the fragility curves previously discussed. The curve was obtained by weighting the  $\mu_D$ -PGA curve of each building typology, for each PGA level, using the weights for the case of larger city (Table 2). This curve was used to associate PSH rates of exceedance of PGA to mean damage levels, according to the procedure discussed in Rota and Rosti (2017). Figure 11 (left) shows the hazard curves produced by Carbon et al. (2012) for Annecy, for different percentiles of the logic tree used for PSH. The obtained PSH rates of exceedance of mean damage levels, for the different percentiles, are reported in Fig. 11 (right).

Figure 12 shows a comparison of the empirically-derived rates of exceedance of mean damage thresholds with PSH estimates. In the figure, dark-grey corresponds to the best estimate of the empirically-derived rates of exceedance, whilst the upper and lower 90% confidence bounds are indicated in black and light-grey, respectively. Diamonds correspond to the average, circles to the median, whilst the error bars represent the variability within the different Monte Carlo runs (i.e. 5th and 95th percentiles).

Starting from a mean damage level equal to 1, PSH predictions are consistent with the best estimate of empirically-derived rates of exceedance, as the latter fall within the different curves derived from PSH. At lower mean damage levels, PSH predictions seem to overestimate results from historical observations, possibly because low intensity observations may not be reported in the seismic catalogue. Furthermore, smaller uncertainty on the best estimate of empirically-derived rates is observed at lower mean damage levels,

**Fig. 10** Weighted mean damage versus PGA curve for the site of Annecy, accounting for the diffusion of the four considered building typologies

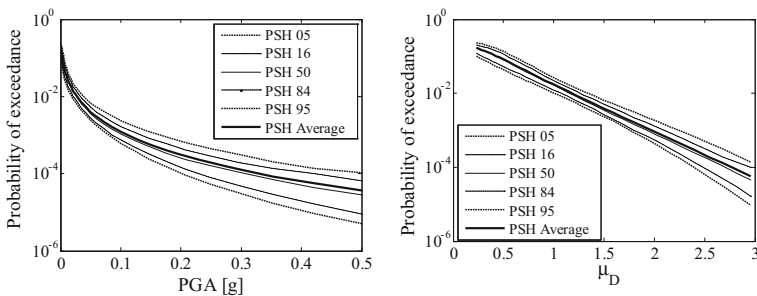
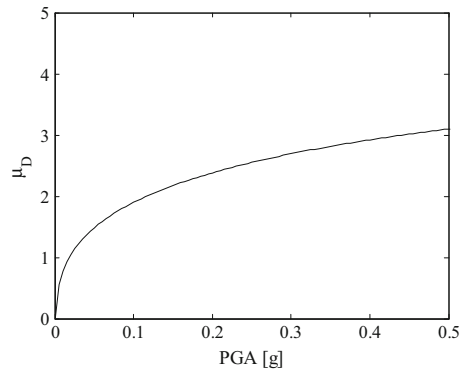
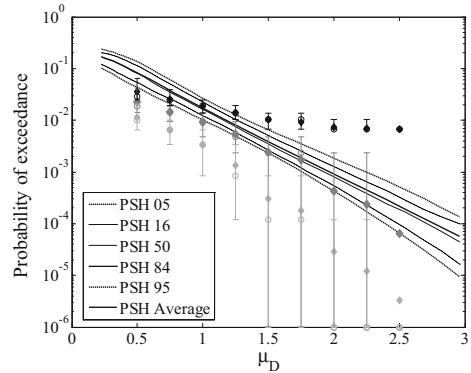


**Fig. 11** PSH curves for different percentiles (5th, 16th, 50th, 84th, 95th and average) (left) and rates of exceedance of mean damage levels (right), for the site of Annecy

**Fig. 12** Comparison of different percentiles of PSH estimates with statistics of the best estimate (dark grey) and of the upper (black) and lower (light grey) 90% confidence bounds of empirically-derived rates of exceedance of mean damage levels, for the site of Annecy. Diamonds average, circles median, error bars 5th and 95th percentiles



whereas it increases at higher  $\mu_D$  thresholds. This could be due to the significant number of low mean damage values resulting from the implementation of the logic tree approach, hence allowing to reach higher confidence on the best estimate at lower  $\mu_D$  levels. Despite the consistency of the results, it appears evident that the dispersion in the empirically-derived rates of exceedance is too large.

The results obtained are obviously affected by the assumptions on the building typologies constituting the building stock at the time of the events and the adopted fragility curves. Their reliability could be hence increased whenever more detailed information would be available. Nevertheless, the aim of this case study is to show a possible application of the methodology presented in Rota and Rosti (2017) and therefore the achieved preliminary results are not themselves the main contribution of this work.

## 5.2 Effect of different sources of uncertainty on the results of the comparison at the site of Annecy

One possible strength of the proposed methodology for converting macroseismic intensities into mean damage values is the opportunity of considering different epistemic uncertainties (i.e. uncertainty in the macroseismic intensity values, in the subdivision of the building stock and in the attribution of the building typologies to the different EMS-98 vulnerability classes). As expected, taking into account several sources of uncertainty led to highly-scattered results. The effect of the different sources of uncertainty on the results of the comparison at single sites was hence investigated, with reference to the site of Annecy.

The first considered source of uncertainty regards the adoption in the macroseismic method of five vulnerability indices, for each building typology, to account for the attribution of the typologies to the different EMS-98 vulnerability classes. Figure 13 shows a comparison of the results obtained by considering the five values of vulnerability index (left) and only one vulnerability index, namely  $V_{50}$  (centre) or  $V_{98}$  (right). As expected, the best estimate of the empirically-derived annual probability of exceedance of  $\mu_D$  levels (dark grey markers) tends to be lower when only vulnerability index  $V_{50}$  is considered and tends to be higher if only  $V_{98}$  is considered. For the case of  $V_{50}$  only, the values of mean damage resulting from the conversion of intensities are also lower, hence limiting the comparison with PSH curves up to values of  $\mu_D$  equal to 1.75. Also, the dispersion in the empirically-derived rates is more reduced in case only  $V_{50}$  is used, whereas it is only slightly reduced when only  $V_{98}$  is selected.

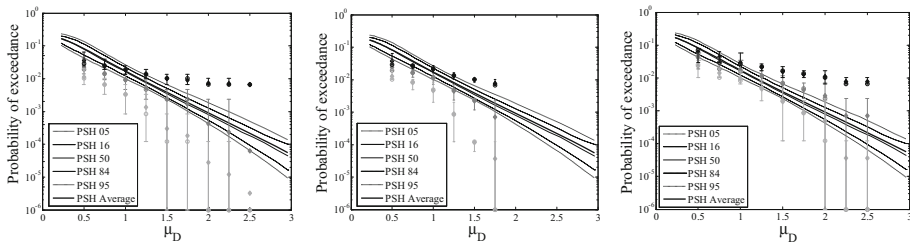


**Fig. 13** Effect of uncertainty in the attribution of the building typologies to the different EMS-98 vulnerability classes: results obtained considering five vulnerability indices (*left*), only vulnerability index  $V_{50}$  (*centre*) and only  $V_{98}$  (*right*)

The effect of the assumed subdivision into building typologies of the building stock at the time of the events was subsequently investigated. Figure 14 (*left*) shows the results obtained by considering the four building typologies of Table 1, with the relative diffusion indicated in Table 2. Figure 14 (*right*) shows instead the results obtained by assuming that the building stock of Annecy is entirely constituted by buildings belonging to typology 2. By comparing the two cases, it can be noted that the dispersion in the results is of the same order of magnitude, indicating that the effect of the uncertainty in vulnerability indices is probably more significant than that deriving from the identification of the more relevant building typologies. The best estimate of the empirically-derived annual rates of exceedance tends to be lower when only typology 2 is considered, probably due to the lower mean damage values corresponding to the vulnerability indices of typology 2, with respect to other typologies (e.g. typology 4).

## 6 Comparison for aggregated sites

### 6.1 Preliminary remarks

The application shown in the previous section for the site of Annecy confirmed that site-specific comparisons are strongly affected by the seismic history of the selected sites.

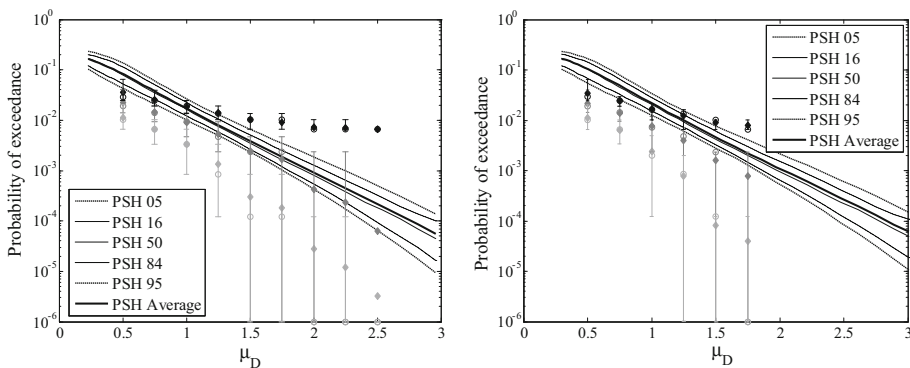


**Fig. 14** Effect of uncertainty in the subdivision of the building stock into different building typologies: results obtained by considering all four building typologies (*left*) and considering only typology 2 (*right*)

Hence, in many cases, the lack of significant macroseismic observations (either in terms of quantity, severity or reliability) may prevent pertinent comparisons with PSH estimates. Indeed, applications to single sites located in South-East France that are not reported in this paper showed that, in many cases, the limited number of macroseismic observations of sufficient entity leads to values of mean damage too small to allow any comparison. For these reasons, a procedure for aggregating multiple sites was developed and discussed in Rota and Rosti (2017). This section proposes an application of this methodology to South-East France, both for the case in which sites are assumed to be affected by independent seismic events and for the case in which this assumption is avoided.

### 6.2 Comparison for aggregated sites assuming independence

Seven sites located in the South-East French territory were selected, consisting of Annecy, Albertville, Draguignan, Beaumont de Pertuis, Digne, La Mure and L'Argentières La Bessée. These sites are assumed to be sufficiently far from each other (see table within Fig. 15), so that exceedances at the different sites could be assumed to be generated by stochastically independent seismic events. Figure 15 shows the seismic history of each site, accounting for uncertainty in the intensity levels reported in SisFrance, and a table showing the geodetic distance (in km) between each couple of sites.

A category of environmental context was assigned to each site, to select weights to be attributed to each building typology based on their (assumed) relative diffusion (Table 2). In particular, Annecy and Draguignan were considered as larger cities, Albertville and La Mure as villages in the Alps, whereas the other three sites were assumed to be smaller villages. Figure 16 shows the equivalent mean damage history of each site, resulting from the application of the logic tree approach for converting intensities into mean damage values.

Mean damage values were then sampled from the equivalent  $\mu_D$  histories through a Monte Carlo approach. Dependent observations (i.e. generated by the same seismic event at the different sites) were checked and eventually removed. The observed number of sites with exceedance was then computed for each selected  $\mu_D$  level. On the other side of the comparison, the predicted number of sites with exceedance was derived, together with

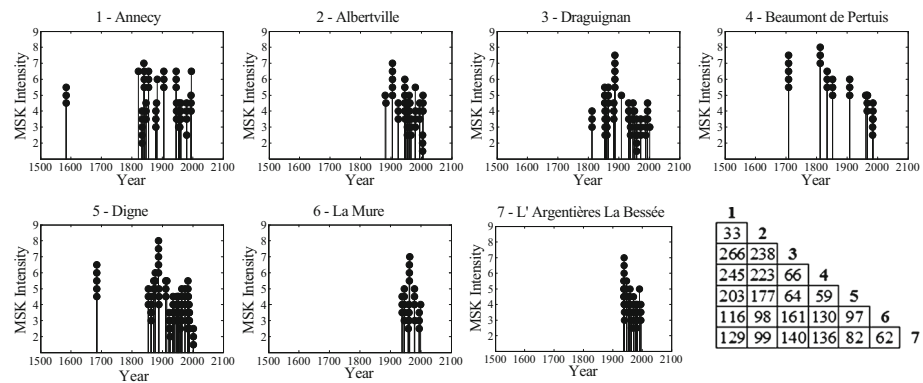


**Fig. 15** Seismic history of the seven considered sites accounting for uncertainty in the intensity values and geodetic distance (in km) between the sites (identified by bold numbers)



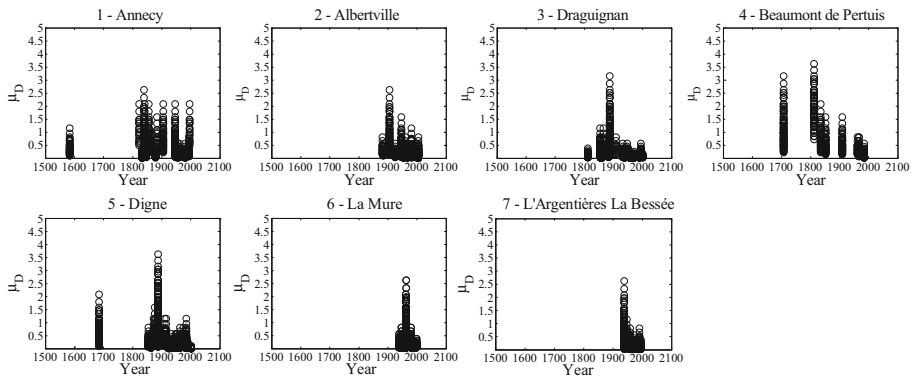


**Fig. 16** Equivalent mean damage history of the seven selected sites

meaningful statistics. The results obtained for the selected set of aggregated sites are shown in Fig. 17.

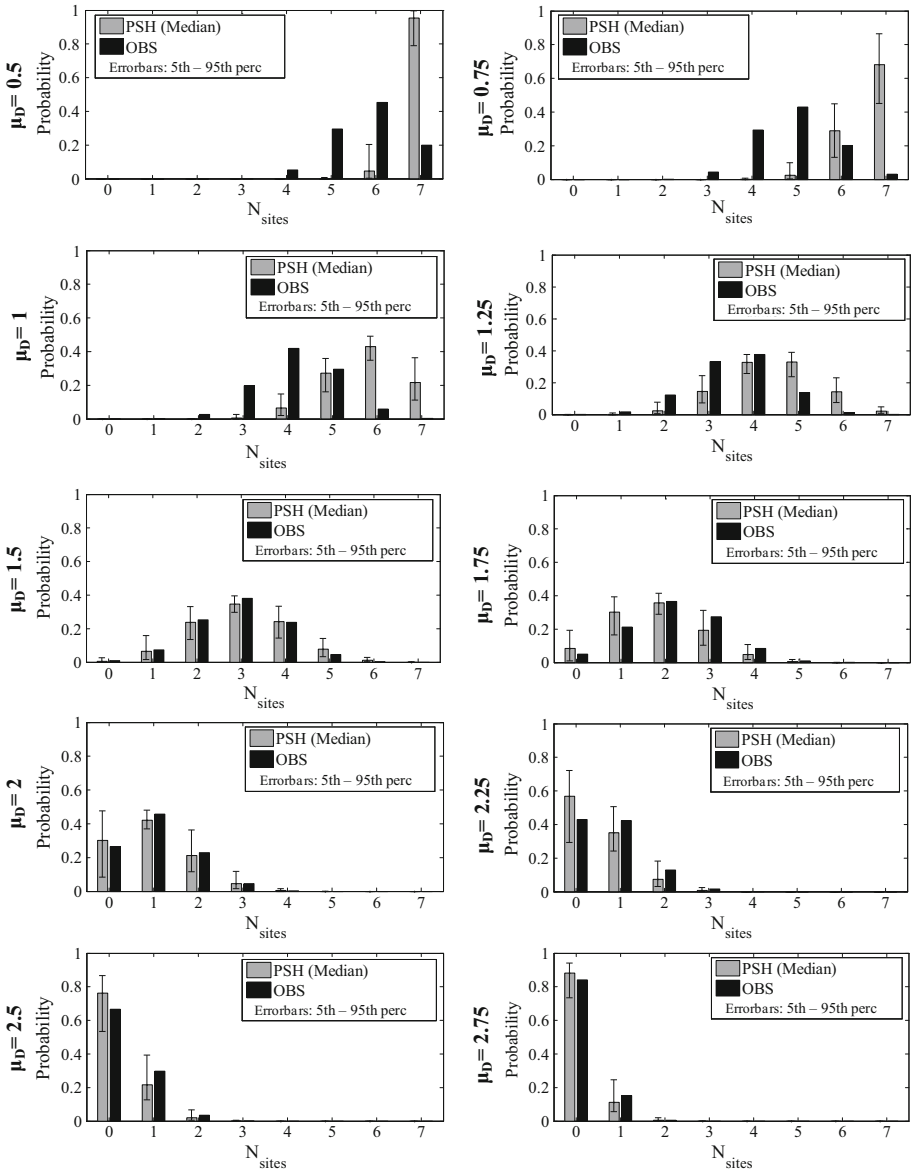
It can be observed that PSH results are consistent with observations starting from a  $\mu_D$  level equal to 1.5, since empirical results fall within percentiles of the predicted distributions. The discrepancy of PSH estimates with observations characterising the lowest mean damage levels can be due to possible low intensity observations missing in the catalogue Sisfrance. To this purpose, the quality of estimation of lower ground motion thresholds could be improved by incorporating recorded accelerations in the procedure.

Figure 18 summarises the results obtained. On the left, statistics of the number of sites with exceedance are shown for the different mean damage levels. On the right, the same results are plotted in terms of PGA, with the only aim of giving an idea of the order of magnitude of the PGAs corresponding to the different  $\mu_D$  levels.

### 6.3 Comparison for aggregated sites without assuming stochastic independence

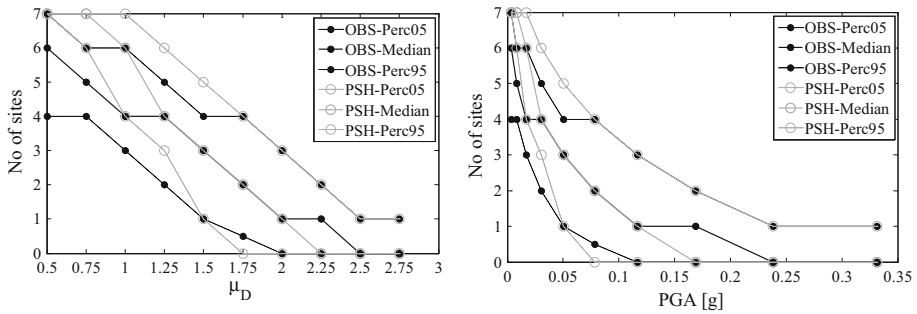
The alternative methodology discussed in Rota and Rosti (2017) was applied as well to the same seven sites. Working in terms of mean annual rates of exceedance in at least one of the selected sites, this procedure allows to avoid the strong assumption on sites' independence, which was instead a requirement of the other methodology.

Figure 19 shows a comparison of the empirically-derived (stars) and the expected (circles) mean annual rates of exceedance in at least one of the selected sites. It can be observed that, starting from a mean damage threshold equal to 1.5, PSH estimates are in agreement with historical observations. Conversely, PSH predictions seem to overestimate empirical results at the lowest mean damage thresholds. In the considered application, the results obtained with this methodology are consistent with those obtained with the other approach, although in the latter case the comparison was carried out in terms of number of sites with exceedance. This seems to suggest that, in this case, the assumption on the stochastic independence does not significantly affect the results. It must be remarked that the comparison of PSH estimates with historical observations seems to be reasonable starting from  $\mu_D$  values larger than 1. Lower mean damage values are indeed derived from macroseismic observations of intensity level at most equal to 6, which are probably less



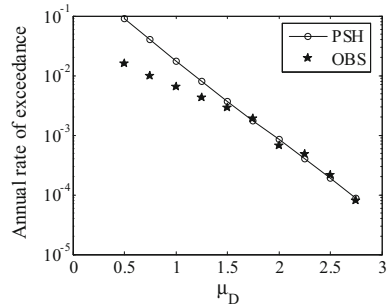
**Fig. 17** Comparison of observed and expected number of sites with exceedance for selected mean damage levels

reliable, and correspond to very low PGAs. Based on these considerations, the preliminary results obtained would indicate that, within the  $\mu_D$  interval of interest (i.e. mean damage levels larger than 1), the consistency of PSH results with historical observations is fairly good for the considered set of sites.



**Fig. 18** Comparison of observed and expected number of sites with exceedance for all mean damage levels (left) and corresponding PGAs (right)

**Fig. 19** Comparison of empirically-derived and PSH-derived annual rates of exceedance in at least one of the seven selected sites



## 7 Comparison at the regional scale

### 7.1 Selection of the area of study

This section illustrates an example of application of the comparison between macroseismic observations and PSH results at a larger scale, considering the entire South-East quarter of France, which includes eleven French departments. Figure 20 shows the sites considered for the comparison at the regional scale level, which consist of 580 of the 858 grid points, approximately distributed at 10 km intervals, for which Carbon et al. (2012) provided PSH estimates. The other points were excluded as they were falling in the Mediterranean Sea or in neighbouring countries (165 points), or because they were located in adjacent French departments (113 points).

### 7.2 Identification of the seismic events and generation of PGA random fields

The proposed methodology is illustrated in detail in Rota and Rosti (2017) and is based on the generation of spatially correlated random fields of PGA, constrained to the available macroseismic intensity observations, to derive distributions of PGA, representing the ground motion that should have been experienced at the considered sites, due to the occurrence of selected seismic events.

PGA random fields were generated for a set of earthquakes, for which synthetic observations were produced at the selected locations. All the independent seismic events producing macroseismic intensity observations at least equal to 4 within the study area

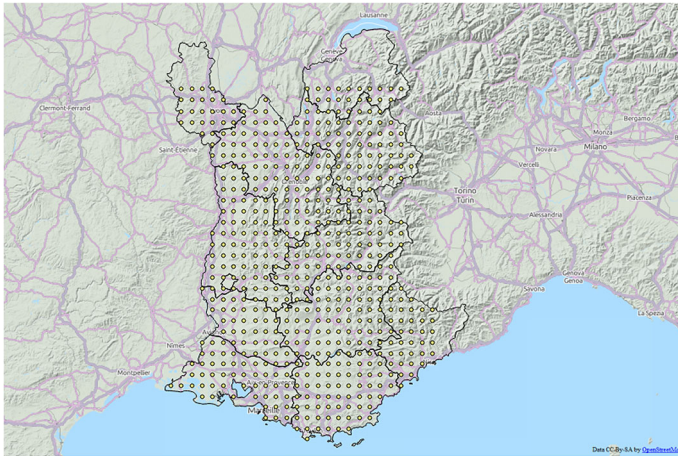
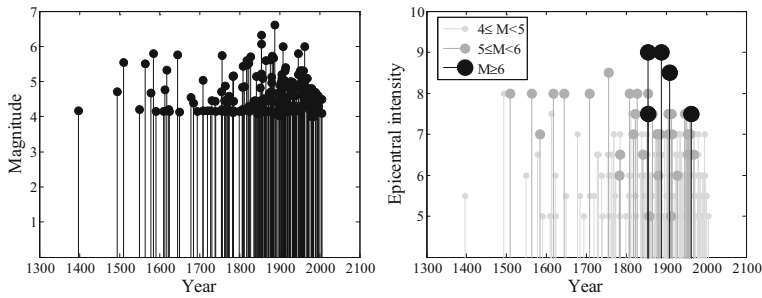


**Fig. 20** Selected grid of sites for the comparison at the regional scale level

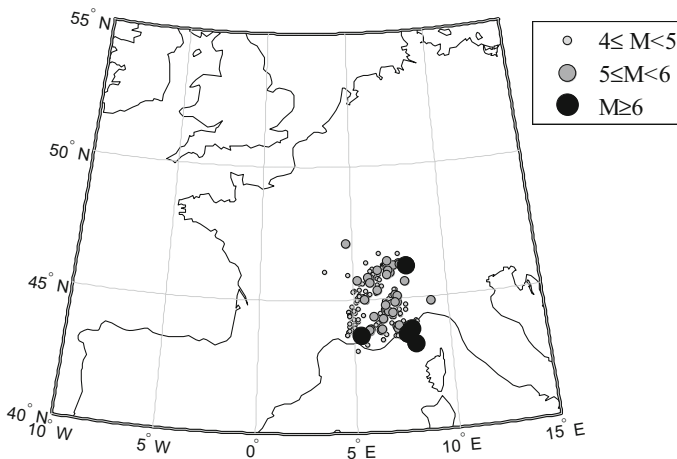
were considered, provided information on the epicentral intensity and magnitude were available. Data on epicentral location and intensity were retrieved from the SisFrance online database, whereas moment magnitude values were collected from the SHEEC catalogue (Stucchi et al. 2013), as they are not reported in SisFrance. Random fields were generated using the Akkar et al. (2014) ground motion prediction equation and the long-range version of the spatial correlation model of Jayaram and Baker (2009). In this preliminary application, a single GMPE was used, although sensitivity analyses on the effect of different GMPEs should have been carried out. Since the selected GMPE is applicable for magnitudes from 4 to 8 and distances up to 200 km, only seismic events with these characteristics were considered. Furthermore, only seismic events with epicentral intensity at least equal to 5 were accounted for, to model only earthquakes that produced some level of damage on buildings. The final dataset used to generate PGA random fields hence included 196 seismic events of magnitude ranging from 4 to 6.62. Since the Akkar et al. (2014) GMPE was developed for moment magnitude, in case of earthquakes for which moment magnitude was not available, the equivalence of local and moment magnitudes was assumed. This is clearly an approximation, as literature works (e.g. Goertz-Allmann et al. 2011, for Switzerland) have shown that the two scales are not equivalent. In the considered magnitude range (from 4 to 6.62), the adopted assumption provides values of moment magnitude overestimated by 0.3 units, with respect to the values proposed by Goertz-Allmann et al. (2011).

Figure 21 (left) shows the years of occurrence of the selected events, with the corresponding magnitude value, whereas Fig. 21 (right) shows the epicentral intensity of each seismic event versus time. The colour and size of the markers depend on the magnitude of the event. Figure 22 shows the epicentral location of each earthquake, with the different colour and size of the markers corresponding to different ranges of magnitude.

No finite fault models or fault type mechanism were available for the calculations and it was therefore decided to adopt the Akkar et al. (2014) model for epicentral source-to-site distances and a default fault mechanism (strike-slip). The use of the epicentral distance model was considered acceptable for most of the modelled events, which are either small earthquakes, for which the difference between distance from the epicentre and distance from the fault can be considered negligible, or larger events (five earthquakes with



**Fig. 21** Magnitude of the selected seismic events versus time (*left*) and epicentral intensity of the selected seismic events versus time (*right*)



**Fig. 22** Location of the epicentres of the selected seismic events, with indication of the magnitude range

$M_w \geq 6$ ), which however occurred far away from the sites of interest. However, the use of a finite fault model could allow to improve the modelled ground motion fields in few cases.

For all the selected earthquakes, the intensity points located at a distance smaller than 100 km from the grid points, with intensity at least equal to 4, were used as a constraint for random fields modelling. Intensity points located farther than 100 km from the sites would have no effect on the results of the simulation, since the effects of spatial correlation of PGA from site to site becomes almost irrelevant already beyond 30 km. Random fields were generated for PGA on rock, consistently with the hazard study to be tested. Site conditions were evaluated based on the  $V_{s,30}$  map produced by USGS (Wald and Allen 2007), available online (<http://earthquake.usgs.gov/hazards/apps/vs30/predefined.php#Europe>). For each considered seismic event, the simulation of PGA random fields provided a lognormal probability distribution of PGA at the considered sites, which is compatible with the characteristics of the event and is conditioned on the available macroseismic observations.

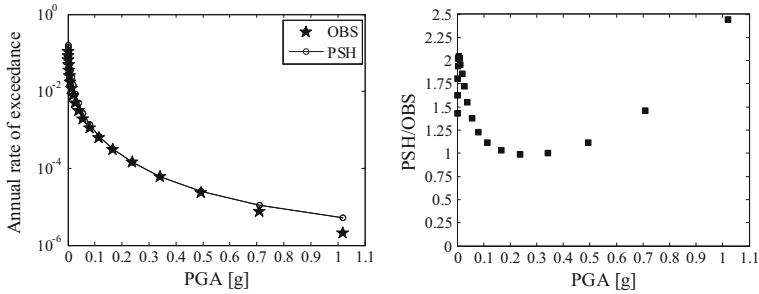


**Fig. 23** Comparison of empirically-derived and PSH-derived annual rates of exceedance in at least one of the sites (*left*) and ratio of PSH-derived over empirically-derived annual rates of exceedance in at least one of the sites (*right*)

### 7.3 Results of the comparison at the regional scale level

The comparison at the regional scale was carried out in terms of empirically-derived and expected annual rates of exceedance of preselected PGA thresholds, in at least one of the selected sites (Fig. 23 left). Empirically-derived rates were obtained by means of PGA random fields, constrained to the available historical observations, whereas expected rates were derived from the results of the considered PSH study. In the figure, stars correspond to observations, whereas the line with circles corresponds to PSH estimates.

Also thanks to the logarithmic scale adopted in the plot, the comparison seems to provide very close results in the entire PGA range. To better explore the consistency of the obtained rates of exceedance, the ratio of PSH over empirically-derived rates of exceedance was calculated, as shown in Fig. 23 (right). In almost all cases, the ratio was higher than 1, suggesting the tendency of PSH estimates of overestimating empirical results. In the 0.1–0.5 g PGA range, the ratio was approximately equal to 1, indicating a good agreement between PSH predictions and observations. The overestimation at lower PGA levels may be explained by the exclusion of seismic events with lower epicentral intensity and magnitude values from the list of events considered for the generation of random fields, although it is believed that these events would not significantly affect the results.

## 8 Conclusions

This paper presented several examples of application of the methodology proposed in Rota and Rosti (2017) for the comparison of PSH results against macroseismic observations. The area of study was the South-East quarter of France and it was selected because of the interest of the scientific and industrial French community on improving the knowledge on PSH methodologies and the reliability of PSH results.

South-East France is a moderate seismicity region with a long history of civilization, hence characterised by a relatively long history of macroseismic observations, which are collected in the online seismic catalogue SisFrance. The statistical analyses carried out on both events and macroseismic observations for the study area showed that the available macroseismic data of relevance for the comparison with PSH results are rather scarce. Indeed, although a very significant number of events is reported in SisFrance, with many associated macroseismic observations, only a small percentage of the available

observations has an intensity level at least equal to 6, corresponding to slight damage on structures (according to the MSK scale). Therefore, the seismic history of most sites located in the region highlighted a very limited number of observations corresponding to some structural damage and this was obviously reflected in the results of the comparison at single sites. Although the site considered in this paper (Annecy) was one of those with the largest number of macroseismic observations with intensity level at least equal to 6, the comparison produced highly scattered results, due to the reduced number of observations producing mean damage values of interest. This large scatter in the results was also due to the fact that the proposed methodology takes into consideration several sources of uncertainty, whose effect on the results for the site of Annecy was investigated.

The comparison at a single site is unavoidably affected by the seismic history of the sites. For the case of South-East France, the limited number of macroseismic intensities of engineering interest may represent an issue, preventing pertinent comparisons with PSH results and significantly limiting the range of mean damage values for which the comparison is meaningful. In these cases, the adoption of a larger scale for the comparison has the advantage of significantly enlarging the size of the available macroseismic dataset, by aggregating the information available at single sites. The drawback is that, both considering a set of aggregated sites and extending the procedure to the entire regional level, the results only allow to test the consistency of PSH results with observations in average terms, without providing any specific information for single sites.

An important issue to be properly considered regards the stochastic dependency of observations at the different sites. This paper reports two examples of application of the comparison for a set of seven aggregated sites, either assuming the observations were generated by independent events and removing this hypothesis. In this specific example, the two cases provided similar results, according to which PSH results turned out to be consistent with empirical observations above a mean damage level approximately equal to 1.5, whereas the empirical results were overestimated at lower mean damage levels. This overestimation could be partially explained by the possible lack of low intensity observations in the catalogue SisFrance. In this case, the incorporation of recorded accelerations in the procedure could improve the quality of estimation of lower ground motion thresholds. The results obtained for the set of seven sites were encouraging and suggested the opportunity of extending the comparison to the entire region of interest. Even in this case, the results confirmed the generally good agreement between PSH predictions and observations for South-East France.

It is important to remark that the aim of this work was to show the applicability and feasibility of the methodology proposed in Rota and Rosti (2017), to the challenging case study of South-East France, i.e. a moderate seismicity region with a limited number of macroseismic observations. The results obtained are only preliminary and they are obviously affected by the different assumptions used. The availability of more detailed information and further investigations on specific aspects could allow the attainment of more reliable results and accurate comparisons with PSH.

**Acknowledgements** This work was developed within the framework of the Project SIGMA, under the financial support of Areva. The authors would like to acknowledge Mr. J.M. Thiry of Areva, Dr. G. Senfaute of EDF, Dr. Ch. Martin of Geoter, and Prof. P. Bazzurro of Istituto Universitario di Studi Superiori (IUSS) Pavia for several discussions on the topic. Very helpful revisions of a previous version of the work carried out in the SIGMA project were provided by Prof. E. Faccioli, Dr. A. Gurpinar, Dr. G. Woo and Dr. J. Savy. Special acknowledgements are due to Dr. E. Fiorini of EUCENTRE, for her work on the application of the methodology at the regional scale, to Dr. Sonia Giovinazzi for her help with the application of the macroseismic method and to Prof. A. Penna and Prof. G. Magenes for their fundamental help at different



phases of the work. The fragility curves adopted in the work were derived with the financial support of the Department of Civil Protection, within several operational research projects of Eucentre and Reluis.

## References

- Akkar S, Sandikkaya MA, Bommer JJ (2014) Empirical ground-motion models for point- and extended-source crustal earthquake scenarios in Europe and the Middle East. *Bull Earthq Eng* 12(1):359–387
- Albarelo D, D'Amico V (2008) Testing probabilistic seismic hazard estimates by comparison with observations: an example in Italy. *Geophys J Int* 175:1088–1094
- Baker JW, Abrahamson NA, Whitney JW, Board MP, Hanks TC (2013) Use of fragile geologic structures as indicators of unexceeded ground motions and direct constraints on probabilistic seismic hazard analysis. *B Seismol Soc Am* 103(3):1898–1911
- Beauval C (2011) On the use of observations for constraining probabilistic seismic hazard estimates—brief review of existing methods. In: International conference on applications of statistics and probability in civil engineering, Zurich, Switzerland
- Braga F, Dolce M, Liberatore D (1982) A statistical study on damaged buildings and an ensuing review of the MSK76 scale. In: 7th European conference on earthquake engineering, Athens, Greece
- Carbon D, Drouet S, Gomes C, Leon A, Martin Ch, Secanell R (2012) Initial probabilistic seismic hazard model for France's southeast ¼. Inputs to SIGMA Project for tests and improvements. Deliverable SIGMA-2012-D4-41, Final Report
- Goertz-Allmann BP, Edwards B, Bethmann F, Deichmann N, Clinton J, Fäh D, Giardini D (2011) A new empirical magnitude scaling relation for Switzerland. *Bull Seismol Soc Am* 101(6):3088–3095
- Grünthal G, Musson RMW, Schwarz J, Stucchi M (1998) European Macroseismic Scale 1998. Cahiers du Centre Européen de Géodynamique et de la Seismologie, Conseil de L'Europe, vol 15. Luxembourg
- Gruppo di lavoro CPTI (2004) Catalogo Parametrico dei Terremoti Italiani, versione 2004 (CPTI04). INGV, Bologna. doi:[10.6092/INGV.IT-CPTI04](https://doi.org/10.6092/INGV.IT-CPTI04)
- Iervolino I (2013) Probabilities and fallacies: why hazard maps cannot be validated by individual earthquakes. *Earthq Spectra* 29(3):1125–1136
- Jayaram N, Baker JW (2009) Correlation model for spatially distributed ground-motion intensities. *Earthq Eng Struct Dyn* 38(15):1687–1708
- Labbé PB (2010) PSHA outputs versus historical seismicity example of France. In: 14th European conference on earthquake engineering, Ohrid, Macedonia
- Lagomarsino S, Giovinazzi S (2006) Macroseismic and mechanical models for the vulnerability and damage assessment of current buildings. *Bull Earthq Eng* 4:415–443
- Levenberg K (1944) A method for the solution of certain non-linear problems in least squares. *Q Appl Math* 2(2):164–168
- Locati M, Camassi R, Stucchi M (eds) (2011) DBMI11, the 2011 version of the Italian macroseismic database. Istituto Nazionale di Geofisica e Vulcanologia, Milano, Bologna. <http://emidius.mi.ingv.it/DBMI11>
- Marquardt DW (1963) An algorithm for the least-squares estimation of nonlinear parameters. *SIAM J Appl Math* 11(2):431–441
- Medvedev S, Sponheuer W, Karnik V (1964) Neue seismische Skala Intensity scale of earthquakes, 7. Tagung der Europäischen Seismologischen Kommission vom 24.9. bis 30.9.1962. In: Jena, Veröff. Institut für Bodendynamik und Erdbebenforschung in Jena, vol 77. Deutsche Akademie der Wissenschaften zu Berlin, pp 69–76
- Ordaz M, Reyes C (1999) Earthquake hazard in Mexico City: observations versus computations. *Bull Seismol Soc Am* 89(5):1379–1383
- Purvance MD, Brune JN, Abrahamson NA, Anderson JG (2008) Consistency of precariously balanced rocks with probabilistic seismic hazard estimates in Southern California. *Bull Seismol Soc Am* 98(6):2629–2640
- Riedel I, Guéguen Ph, Dalla Mura M, Pathier E, Leduc T, Chanussot J (2015) Seismic vulnerability assessment of urban environments in moderate-to-low seismic hazard regions using association rule learning and support vector machine methods. *Nat Hazards* 76(2):1111–1141
- Rosti A, Rota M, Penna A, Magenes G (2017) Statistical treatment of empirical damage data collected after the main Italian seismic events (1980–2009). In: Proceedings of 16th world conference on earthquake engineering, Santiago, Chile
- Rota M, Rosti A (2017) Comparison of PSH results with historical macroseismic observations at different scales. Part 1: methodology. *Bull Earthq Eng*. doi:[10.1007/s10518-017-0157-z](https://doi.org/10.1007/s10518-017-0157-z)



- Rota M, Penna A, Strobbia CL (2008a) Processing Italian damage data to derive typological fragility curves. *Soil Dyn Earthq Eng* 28(10–11):933–947
- Rota M, Penna A, Strobbia C, Magenes G (2008b) Derivation of empirical fragility curves from Italian damage data. Research Report No. ROSE-2008/08, IUSS Press, Pavia, ISBN: 978-88-6198-029-7, p 240
- Rovida A (2013) The Italian macroseismic database (DBMI11) at the Italian–French border. In: Workshop macroseismicity: sharing and use of historical data, 3 April 2013, Paris
- Sabetta F, Pugliese A (1987) Attenuation of peak horizontal acceleration and velocity from Italian strong-motion records. *Bull Seismol Soc Am* 77(5):1491–1513
- Scotti O (2013) Joining forces/efforts to improve our knowledge of the effects of earthquakes affecting France and neighbouring countries. In: Workshop macroseismicity: sharing and use of historical data, Paris
- Scotti O, Baumont D, Quenet G, Levret A (2004) The French macroseismic database SISFRANCE: objectives, results and perspectives. *Ann Geophys* 47(2–3):571–581
- Sisfrance – Catalogue des séismes français métropolitains, BRGM, EDF, IRSN. <http://www.sisfrance.net>
- Stein S, Geller R, Liu M (2011) Bad assumptions or bad luck: why earthquake hazard maps need objective testing. *Seismol Res Lett* 82(5):623–626
- Stirling M (2012) Earthquake hazard maps and objective testing: the Hazard Mapper’s point of view. *Seismol Res Lett* 83(2):231–232
- Stirling M, Gerstenberger M (2010) Ground motion-based testing of seismic hazard models in New Zealand. *Bull Seismol Soc Am* 100(4):1407–1414
- Stirling M, Petersen M (2006) Comparison of the historical record of earthquake hazard with seismic-hazard models for New Zealand and the continental United States. *Bull Seismol Soc Am* 96(6):1978–1994
- Stucchi M, Rovida A, Gomez Capera AA, Alexandre P, Camelbeeck T, Demircioglu MB, Gasperini P, Kouskouna V, Musson RMW, Radulian M, Sesetyan K, Vilanova S, Baumont D, Bungum H, Fäh D, Lenhardt W, Makropoulos K, Martinez Solares JM, Scotti O, Živčić M, Albin P, Batllo J, Papaioannou C, Tatevossian R, Locati M, Meletti C, Viganò D, Giardini D (2013) The SHARE European Earthquake Catalogue (SHEEC) 1000–1899. *J Seismol* 17(2):523–544
- Tasan H, Beauval C, Helmstetter A, Sandikkaya A, Guéguen Ph (2014) Testing probabilistic seismic hazard estimates against accelerometric data in two countries: France and Turkey. *Geophys J Int* 198(3):1554–1571
- Wald DJ, Allen TI (2007) Topographic slope as a proxy for seismic site conditions and amplification. *Bull Seismol Soc Am* 97(5):1379–1395
- Ward SN (1995) Area-based tests of long-term seismic hazard predictions. *Bull Seismol Soc Am* 85(5):1285–1298